

## An optimal fitting approach to improve the GISS ModelE aerosol optical property parameterization using AERONET data

Jing Li,<sup>1,2</sup> Li Liu,<sup>2</sup> Andrew A. Lacis,<sup>2</sup> and Barbara E. Carlson<sup>2</sup>

Received 20 January 2010; revised 20 April 2010; accepted 27 April 2010; published 28 August 2010.

[1] We improve the updated 2000 Goddard Institute for Space Studies, New York, ModelE aerosol optical property parameterization using an optimal fitting approach with AERONET ground measurements. The model aerosol optical properties, such as optical depth, are calculated using the aerosol mass density field from a chemical transport model, Mie scattering parameters, a prescribed dry size for each aerosol species assuming external mixing, and a hygroscopicity parameterization. A comparison between the model- and AERONET-measured optical depth (AOD) and Ångström exponent (AE) indicates that the general circulation model (GCM) aerosol parameterization has a flatter AOD spectral dependence, thus a very low biased AE, which suggests that the aerosol sizes used in the model are too large. The seasonal variation of GCM AE also disagrees with that of AERONET data. On the basis of these results, we identify GCM aerosol size as the most poorly constrained parameter and develop an optimal fitting technique to adjust the GCM aerosol dry size by minimizing the total mean square error between the GCM and AERONET AOD at the six AERONET wavelengths. After adjusting the aerosol's dry size, the agreement between the GCM AE with AERONET data is improved. The fitted AOD at the six wavelengths closely matches AERONET data over most biomass burning, dust, and rural regions. The results are also greatly improved for the other aerosol types. The global distribution of the optimally fitted sizes displays regionally uniform characteristics, which allows the generation of a geographically varying size data set. Model uncertainty caused by other factors is also represented by an uncertainty parameter, which is mainly attributed to errors from aerosol mass concentration, Mie scattering parameters, relative humidity, and AERONET measurements. The relative contribution of each of these errors sources depends on the relevant aerosol type. Further comparison between the absorption optical depth and AE spectral dependence provides additional information on absorbing aerosols and GCM fine-to-coarse mode ratio, which will be addressed in future research.

**Citation:** Li, J., L. Liu, A. A. Lacis, and B. E. Carlson (2010), An optimal fitting approach to improve the GISS ModelE aerosol optical property parameterization using AERONET data, *J. Geophys. Res.*, 115, D16211, doi:10.1029/2010JD013909.

### 1. Introduction

[2] Aerosols play important roles in the Earth's radiative balance. They have the direct effect by scattering and absorbing solar radiation and the indirect effect by interacting with water vapor to affect cloud formation and lifetime. Absorbing aerosols also have the semidirect effect by heating the atmosphere layer, reducing cloud fraction, and suppressing convection. However, because of their highly variable spatial and temporal distribution; their direct, indirect, and semidirect effects; and their counteracting effect between absorbing and nonabsorbing aerosols, they have been identified as the largest single source of uncertainty in the

anthropogenic contribution to global forcing of climate change [*Hansen et al.*, 2000, 2002; *Intergovernmental Panel on Climate Change*, 2001].

[3] Global-scale models, which simulate the emission, transport, chemical processes, removal, and radiative properties of aerosols, are extremely useful in assessing the climate impact of aerosols [*Textor et al.*, 2006]. In new aerosol modules, aerosols are generally distinguished among several types, and their mass fields are separately generated from emission sources through a series of highly parameterized processes [*Kinne et al.*, 2003]. Then, aerosol optical properties are calculated by assuming aerosol dry sizes and specifying their scattering and absorption properties. Because aerosol optical properties are directly related to their radiative effects, it is necessary to accurately represent aerosol optical properties in global climate models or general circulation models (GCMs). Previously, *Liu et al.* [2006] validated Goddard Institute for Space Studies, New York (GISS), ModelE aerosol climatology of 1990 by comparing with

<sup>1</sup>Department of Earth and Environmental Sciences, Columbia University, New York, New York, USA.

<sup>2</sup>NASA Goddard Institute for Space Studies, New York, New York, USA.

satellite data from Moderate Resolution Imaging Spectroradiometer (MODIS), Multiangle Imaging Spectroradiometer (MISR), Polarization and Directionality of Earth Reflectances, advanced very high resolution radiometer, and Total Ozone Mapping Spectrometer (TOMS) and ground data from AERONET. Their results reveal an overall low bias in GCM Ångström exponent (AE), suggesting a problem in aerosol size specification. The model intercomparison by *Kinne et al.* [2003] also suggests that the GISS model has comparatively large sizes for sulfate and carbon aerosols. Although the GISS ModelE aerosol mass fields have been updated, the assumed dry sizes remain unchanged. As a result, the purpose of this work was to adjust GCM aerosol dry size through comparing and matching with AERONET spectrally dependent AOD data.

[4] The setup of aerosol modules, either GCMs or chemical transport models, generally consists of two parts: chemical transport model, which simulates the emission, evolution, and transport of aerosols and generates the mass density field for each aerosol species on a decadal scale; and radiative transfer model, which converts the mass density into optical properties by defining aerosol size and specifying their Mie scattering parameter and hygroscopicity. A detailed description of the GISS GCM is given in section 2. On the basis of comparison studies such as that of *Liu et al.* [2006] and improved knowledge on aerosol processes, the GISS GCM tropospheric aerosol mass concentration field has been updated from 1990 to 2000 [*Koch et al.*, 2006, 2007; *Bauer et al.*, 2007]. Dust climatology has also been updated by *Miller et al.* [2006]. This new aerosol field shows improvements from the previous simulation, such as enhanced sulfur emission at remote locations, use of a wind-based parameterization for sea salt [*Koch et al.*, 2006], reduced scatter and bias in black carbon distribution [*Koch et al.*, 2007], and improved dust transport over the Atlantic [*Miller et al.*, 2006]. Using this updated aerosol mass density field, in this study, we concentrate on the radiation model and compare aerosol optical properties to observation. We also make further attempts to adjust parameters in the mass density, such as optical depth conversion process, and to investigate model uncertainties. Aerosol optical properties and hence their radiative effects are determined by the aerosol size distribution and mass concentration of the various components. In the parameterization of the radiation model, aerosol size is considered to be the largest source of uncertainty, mainly because the GCM assumes a fixed dry size for the five major tropospheric aerosols. These sizes are generally empirical and prove to be problematic by comparing with observation data. Uncertainty in aerosol size specification is a common problem for most GCMs. *Kinne et al.* [2003] compared the aerosol properties in seven climate models and found that different models can have very different aerosol dry size specification. For example, dry aerosol sizes for organic carbon aerosols used in these models range from 0.02 to 0.50  $\mu\text{m}$ , black carbon aerosol sizes range from 0.02 to 0.10  $\mu\text{m}$ , and sulfate aerosol sizes range from 0.12 to 0.30  $\mu\text{m}$ . Also, some models may have more than one mode for a certain aerosol species. Their comparison of assumed dry sizes in each model indicates that the GISS model has larger sulfate, black carbon, and organic carbon aerosol sizes. This results in errors in the conversion of aerosol mass into optical depth, which will further influence the accuracy of aerosol radiative forcing

calculations. Moreover, the treatment of aerosol mixing also varies from completely internally mixed to completely externally mixed [*Textor et al.*, 2006]. However, only limited attempts have been made to improve aerosol size specification in models. *Lesins and Lohmann* [2003] used spectrally dependent AE data from AERONET measurements to deduce a geographically varying aerosol size distribution in the CCCma GCM. They further generated an aerosol size data set for the ECHAM4 climate model on the basis of the fine-mode aerosol optical depth (AOD) fraction derived from MODIS and AERONET [*Lesins and Lohmann*, 2005]. Unlike GISS ModelE, which assumes external aerosol mixing, their aerosols are assumed to have only two internally mixed modes for the fine and coarse size classes. No work has been done on the improvement of externally mixed aerosol sizes based on available observations. As a result, our primary objective was to adjust the aerosol dry size parameterization to better match model and measured aerosol optical properties. This goal is achieved by adopting an optimal fitting approach to minimize the mean square error (MSE) between the seasonal cycles of GCM and AERONET AOD at available AERONET wavelengths. The remaining errors are largely attributed to errors in the aerosol mass concentration generated by the chemical transport model and Mie scattering parameters, which, at present, is beyond the scope of this research. Furthermore, as indicated in the study of *Textor et al.* [2006, Table 2], the majority of the 16 AeroCom aerosol modules assume external aerosol mixing, and the method and results presented here can be extended to other models rather than confined with the GISS GCM.

[5] There are several reasons for using AERONET data to improve aerosol model parameterization. First, this is the most complete ground-based network of aerosol measurements, with wide spatial coverage and high data quality. Second, AERONET instruments directly measure aerosol extinction from the surface, exempt from the need to assume surface reflectivity and single-scatter albedo, which are major sources of uncertainty for satellite retrievals of aerosol properties. *Mishchenko et al.* [2007] compared aerosol climatology between MODIS-Aqua, MODIS-Terra, MISR, and GACP and found significant differences that exceed the corresponding individual uncertainty claims. *Liu and Mishchenko* [2008] further compared MODIS and MISR level 2 aerosol products at pixel resolution. Again, their results showed a worse-than-expected correlation between ocean AOD and essentially no correlation between the AEs. Both studies suggest limitations and problems in satellite data. Third, AERONET Sun photometers typically have seven channels: 340 nm, 380 nm, 440 nm, 500 nm, 675 nm, 870 nm, and 1020 nm, which provides additional information regarding aerosol size and composition.

[6] To facilitate comparison and to take advantage of the AOD spectral information, we begin by constructing an “AERONET simulator” within the GCM to simulate clear-sky column AOD at six AERONET wavelengths. The 1020 nm channel is not used because of possible contaminations by water vapor. Next, from the results, we identify aerosol size as the most poorly constrained parameter in the optical property calculation within the radiation model and develop an optimal fitting technique to find the best size combination of sulfate, nitrate, organic carbon, black carbon, and sea-salt aerosols. Dust aerosol sizes are excluded from

the fitting because they already have seven size bins. The fitted model aerosol optical properties show significant improvements. Furthermore, the fitting procedure generates an improved geographically varying aerosol size field that can be readily applied in the radiation model. It also helps to quantify possible errors from the chemical transport model, aerosol Mie parameters, and the ambient relative humidity.

[7] The paper is organized as follows: in section 2, we describe the new GCM aerosol climatology; in section 3, we briefly introduce the AERONET data used in this study; in section 4, we present the comparison results between the GCM and AERONET for five major aerosol types namely, dust, biomass burning, maritime, urban, and rural; in section 5, we introduce the optimal least squares fitting method to constrain aerosol size and quantify model uncertainty and we present the results; in section 6, we present some discussion following the results; and finally, in section 7, we provide the summary and conclusions.

## 2. GISS ModelE Aerosol Climatology

[8] In this study, we use the updated ModelE 2000 aerosol climatology, which is currently the most updated version. The major tropospheric aerosol species include sulfate, sea salt, black carbon, organic carbon, nitrate, and dust. The distribution of the first five species is from the GISS chemical transport model simulations that define the spatial and time dependence of tropospheric aerosols in the form of monthly mean height-dependent aerosol mass density distributions [Koch, 2001]. The dust field is generated by a dust model embedded within ModelE in the form of monthly mean optical depth with seven size bins [Miller *et al.*, 2006]. The aerosol mass concentration field is simulated on a decadal scale rather than for each specific year, and data for the years within a decade need to be interpolated. The model horizontal resolution is  $4^\circ$  by  $5^\circ$ , and the vertical resolution has been increased from the previous 9 layers to 20 layers.

[9] More specifically, the sulfate emissions for present-day anthropogenic sources are from the Emission Database for Global Atmospheric Research v3.2 [Koch *et al.*, 2006]. Black carbon and organic carbon anthropogenic emissions are from Bond *et al.* [2004]. Biomass burning emissions for BC and OC are based on the Global Fire Emission Database v1 model carbon estimates, together with the carbonaceous aerosol emission factors from Andreae and Merlet [2001]. Sea salt production is from the wind speed-dependent formulation for sea salt generation from whitecap bubble bursting by Monahan *et al.* [1986]. In addition, nitrate aerosols are produced from their gaseous precursors, whose emissions are based on anthropogenic emissions for 1995 from the Emission Database for Global Atmospheric Research v3.2 [Bauer *et al.*, 2007]. Dust emission is chosen so that the dust cycles agree optimally with a worldwide compilation of satellite retrievals and surface measurements [Miller *et al.*, 2006]. After specifying their emission, the chemical transport model and dust model are forced by GCM meteorology (wind field, precipitation, etc.) and surface conditions to generate their distribution.

[10] Aerosol optical properties are calculated in ModelE radiative transfer model. The aerosols are approximated as externally mixed. Effective dry radii are prescribed to be 0.2, 0.3, 0.1, 0.3, and  $1.0 \mu\text{m}$  for sulfate, organic carbon, black

carbon, nitrate, and sea salt, respectively. Dust aerosols are divided into seven size bins ranging from 0.1 to  $5.5 \mu\text{m}$ . The radiative properties of hygroscopic aerosols (i.e., sulfate, nitrate, sea salt, and organic carbon) are parameterized on the basis of laboratory measurements [Tang and Munkelwitz, 1991, 1994; Tang, 1996]. They are treated as an external mixture of the dry aerosol and a pure water aerosol of appropriate size, and lookup tables of Mie scattering coefficients are tabulated for different aerosol compositions as functions of size, wavelength, and relative humidities ranging from 0 to 0.999 [Schmidt *et al.*, 2006]. The ModelE aerosol radiative parameters and their spectral dependence are based on rigorous Mie scattering results.

[11] Given the aerosol mass density distribution and composition from the chemical transfer model, effective radius, complex refractive indices, and hygroscopic properties, AOD (also known as  $\tau$ ) can be calculated using [Lacis and Mishchenko, 1995]

$$\tau = \frac{3Q_{\text{ext}}M}{4\rho r_{\text{eff}}}, \quad (1)$$

where  $\rho$  is the specific density of the aerosol,  $Q_{\text{ext}}$  is the extinction efficiency factor at a certain wavelength, and  $r_{\text{eff}}$  is the effective radius (cross section-weighted radius over the size distribution [Hansen and Travis, 1974]). Generally,  $Q_{\text{ext}}$  is at 550 nm. Here, we simulate AERONET measurements by extending the GCM Mie scattering coefficient tables to specifically include six AERONET Sun photometer channels, namely, 340, 380, 440, 500, 675, and 870 nm, for the year 2000. Only clear-sky AOD are taken into account to be consistent with AERONET sampling. It should be noted that the simulator does not produce exactly the same quantity with AERONET data because the periods between the model and measurements are not exactly the same, and the transport of the aerosols is driven by the GCM wind field rather than real-world meteorology conditions.

[12] This study focuses on the radiation part of aerosol simulation, i.e., the process defined by (1).

## 3. AERONET Ground Data

[13] AERONET is a globally dispersed network of automatic sun and sky scanning radiometers, which provides ground-based measurements of aerosol properties at specific geographic locations [Holben *et al.*, 1998]. Aerosol optical depth is measured at seven wavelengths from UV to near IR: 340, 380, 440, 670, 870, and 1020 nm. Uncertainty in AOD measurements is typically 0.01 for  $\lambda > 440 \text{ nm}$  and 0.02 for  $\lambda < 440 \text{ nm}$  [Eck *et al.*, 1999].

[14] In this study, we use level 2 monthly mean AOD data updated until 3 October 2009. The data are cloud-screened and quality-assured [Smirnov *et al.*, 2000]. We take the multiyear overall monthly average of the data from each station to minimize bias. The 440/870 AE is calculated using a linear regression of  $\ln(\tau)$  against  $\ln(\lambda)$  for available wavelengths between the 440 and 870 nm interval to evaluate aerosol size.

[15] Although, currently, there are more than 500 AERONET stations around the globe, the continuity and consistency of their data vary. Therefore, before comparing with GCM, we applied some data quality control strategies. Most of the stations are selected only if they have at least 2 years of

**Table 1.** Fifteen Selected Grid Boxes: Location, Type, and Dominant Aerosol Species

Name	Latitude, °N	Longitude, °E	Aerosol Type
Banizoumbou	14	2.5	Dust (+bio)
Dahkla	22	-17.5	Dust
Dalanzadgad	42	102.5	Dust
PCS	17	102.5	Biomass
Mongu	-14	-22.5	Biomass
Alta_Floresta	-10	-57.5	Biomass
Midway_Island	30	-177.5	Maritime
Tahiti	-18	-147.5	Maritime
Amsterdam_Island	-38	77.5	Maritime
IC	46	7.5	Urban
GCMSW	38	-77.5	Urban
Mexico_City	17	-97.5	Urban
BX	38	117.5	Rural (+urban)
BONDVILLE	42	-87.5	Rural
Sevilleta	34	-107.5	Rural

measurements, and the multiyear overall monthly average of AOD has at least 9 months of data. A few stations are selected manually to represent typical aerosol types, although they do not strictly follow this criterion. In total, 139 stations are selected, and they fall in 97 GCM grid boxes. If there are two or more stations in a GCM grid box, their data are averaged with equal weights. The locations of grid boxes with data are shown in Figure 8. In general, the data coverage is good in North America and Europe moderate in South America, Africa, and East Asia.

[16] Nevertheless, there is question that one or a few AERONET stations are not representative of the whole GCM grid box because of the high spatial variability of aerosols. In another respect, the atmospheric lifetime of aerosols is typically several days during which they can travel thousands of kilometers, although they may undergo physical and chemical changes. Thus, using observations such as AERONET is a useful way to test and constrain the aerosol climatologies from chemical transport models [Sato *et al.*, 2003]. In addition, the score of the majority of the selected sites range from 3 (1000 km) to 1 (300 km) according to the rating of AERONET sites [Kinne, 2008], providing relatively good representation of a 4° by 5° grid. Improvements will be possible when aerosol distributions are simulated with higher resolution and better coverage of ground observations is attained in the future.

[17] Locally, to examine each GCM aerosol species in more detail, 15 grid boxes are selected representing dust, biomass burning, maritime, urban, and rural aerosols from difference regions (3 grid boxes of each type). Of the 15 grid boxes, 11 contain only one AERONET station, and their names are characterized by the AERONET site name. The “PCS” grid boxes represent “Pimai,” “Chulalongkorn,” and “Silpakorn.” The “IC” box represents “Ispra” and “Carpentras.” The “GCMSW” box represents “GSFC,” “COVE,” “MD\_Science\_Center,” “SERC,” and “Wallops.” In addition, the “BX” grid box represents “Beijing” and “XiangHe.” Table 1 lists their locations and aerosol types. Please note that the latitude and longitude indicate the center of the GCM grid box rather than those of the AERONET station.

#### 4. Comparison of Results

[18] The discussion in this section will focus on the selected 15 grid boxes, which represent five major aerosol types.

Results for the other 82 grid boxes are similar so we will not spend much space showing comparisons on a global scale.

#### 4.1. AOD

[19] The scatterplots between the GCM and AERONET AOD at different wavelengths are shown in Figure 1 for the five aerosol types. The  $R$  value indicates the correlation coefficient between the two data sets. It is clearly observed that GCM underestimates biomass burning, rural, and urban aerosol loading, whereas it overestimates dust and maritime aerosols. The GCM achieves high correlation ( $R > 0.8$ ) with AERONET AOD for biomass burning, dust, and rural aerosols, indicating seasonal cycle agreements, which is encouraging in that it suggests the GCM well captures the temporal variability of most aerosol types. However, the correlation between urban and maritime aerosols is relatively low. The low bias in biomass burning and rural aerosols may result from insufficient emission from the chemical transport model. The new dust climatology increased dust emission over the Sahara region. However, the comparison indicates that the increase might be too high. The disagreement in sea salt reveals potential problems in both emission and meteorology conditions that drive aerosol transport. Industrial regions have a mixture of sulfate, nitrate, black carbon, and organic carbon aerosols. Therefore, the simulation is usually more difficult. In addition, to the model, AERONET data could have errors, such as contamination from thin cirrus clouds. Moreover, the range scores are mostly 0 to 1 for urban sites, making them less representative of the whole GCM grid box. These factors also contribute to the differences.

[20] In addition to the scatterplots, Figure 4 allows a more detailed examination into the 15 grid boxes (dashed line and triangles). While the three grid boxes of each aerosol type bare the same characteristics as discussed above, they also have a few individual features. For example, for dust, Banizoumbou and Dalanzadgad AOD are both significantly higher than AERONET at all channels, while Dahkla only has slightly higher AOD at 870 nm. For biomass burning, Mongu and Alta\_Floresta AOD disagree with AERONET mainly during the summer and autumn peaks, while PCS is biased low all year-round. For maritime aerosols, GCM AOD has differences in both the magnitude and seasonal cycle at Midway\_Island and Tahiti. However, the seasonal cycle at Amsterdam\_Island agrees fairly well with AERONET. Because aerosols are highly variable in space, it is understandable that differences exist between regions dominated by the same aerosol type. However, considering their relatively small contribution compared with common features, in this study, we mainly focus on aerosol types rather than specific grid boxes.

[21] Similar results are observed in global comparisons (figure not shown). The GCM well reproduced the distribution of major aerosol species, including dust over the Sahara and the Persian Gulf; biomass burning over South Africa, South America, and Southeast Asia; and urban pollution over East Asia, Northeast America, and Europe. However, the GCM generally have lower AOD over the midlatitudes but higher over the tropical dust regions.

#### 4.2. ÅE

[22] Following Figure 1, it is seen that the difference between GCM and AERONET AOD is generally smaller at

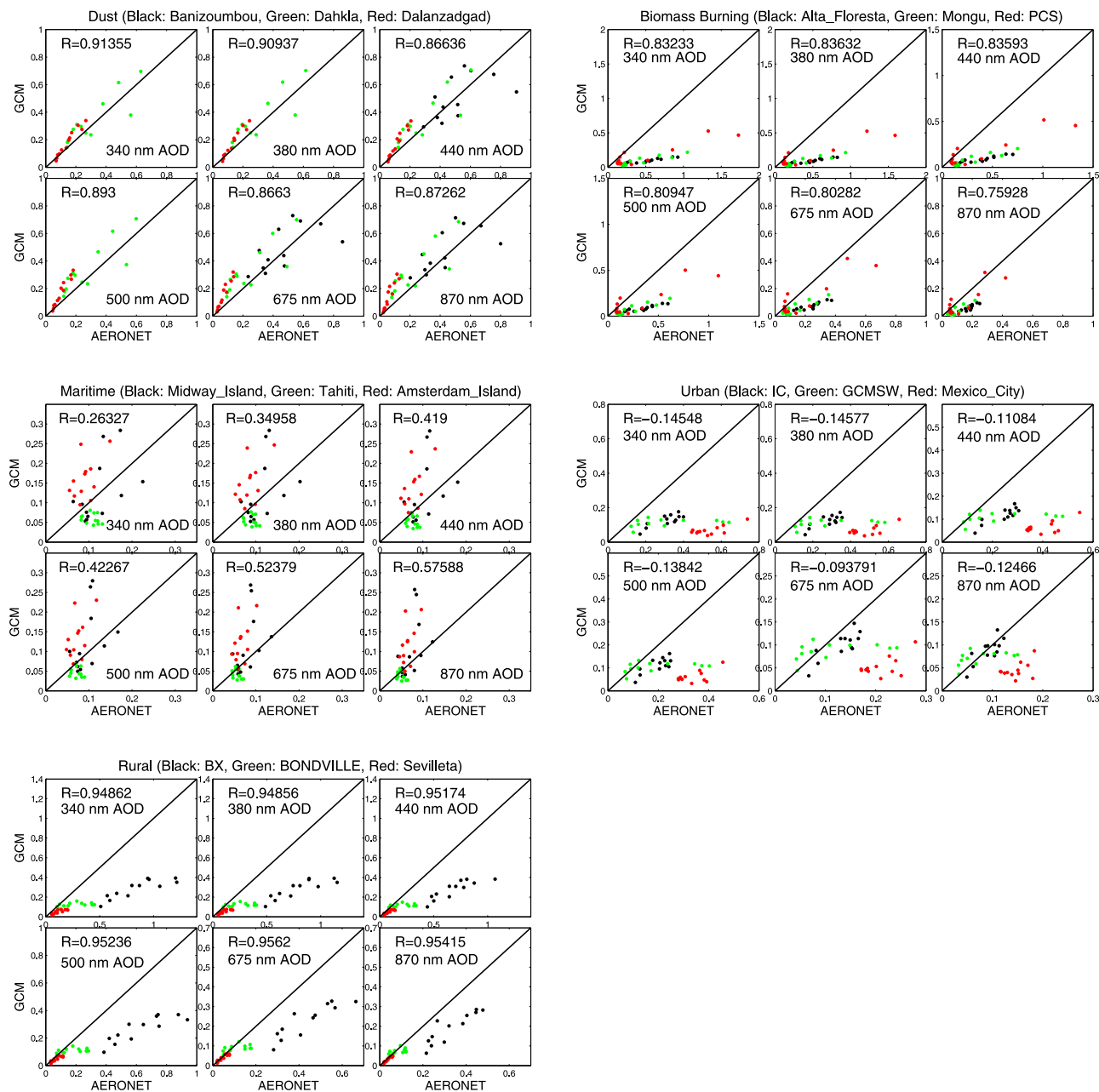


**Figure 1.** Scatterplots of AERONET and GCM AOD and ABS for the five aerosol types. The GCM AOD and ABS are biased low for biomass burning, urban, and rural aerosols but are slightly high for dust and maritime aerosols. Dust, biomass burning, and rural aerosols have high seasonal correlation ( $R$  value) with AERONET. The low seasonal correlation between maritime and urban aerosols indicates problems in sea salt simulation (possibly related to wind field) and the representation of a mixture of sulfate, nitrate, and carbonaceous aerosols.

longer wavelengths, which implies a flatter AOD spectral dependence simulated by the GCM. The spectral dependence of AOD is associated with aerosol size and can be better illustrated with the AE. The Ångström relation is used to parameterize the relationship between aerosol size and dependence of optical depth on wavelength:

$$\tau = \tau_1(\lambda/\lambda_1)^{-\alpha}, \quad (2)$$

where  $\alpha$  is the AE. Larger  $\alpha$  corresponds to smaller particle size.  $\tau$  and  $\tau_1$  are the optical depths at  $\lambda$  and  $\lambda_1$ , respectively. So we have

$$\alpha = -\ln(\tau/\tau_1)/\ln(\lambda/\lambda_1), \quad (3)$$

At least AOD at two wavelengths are required to compute  $\alpha$ . When AOD values at several wavelengths are available,  $\alpha$  can be computed by a linear regression on  $\ln(\tau)$  and  $\ln(\lambda)$ .

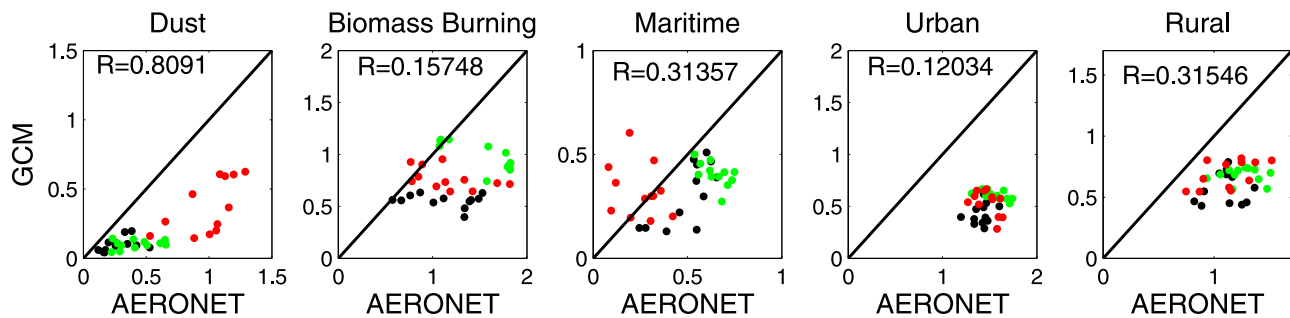


**Figure 2.** Scatterplots of AERONET and GCM AE indicate a lower GCM AE associated with larger aerosol size. The seasonal variability is also poorly reproduced by the GCM except for dust.

[23] In this study, the 440/870  $\alpha$  is obtained using four wavelengths: 440, 500, 675, and 870 nm, and the scatterplot comparison is displayed in Figure 2. We are aware that different errors at different wavelengths in AERONET AOD data may cause biases in AE estimation [Wagner and Silva, 2008]. Therefore, we first carried out a few tests by using AOD data only above certain thresholds (0.07, 0.1, 0.15, and 0.2) and found that the comparison results remain the same (figures not shown). The GCM AE is clearly biased low compared with AERONET for all aerosol types (Figure 2). Moreover, in contrast to AOD, the correlation between the AE is also very low. This feature is most prominent for urban aerosols, where essentially no correlation is observed. Because, currently, the GCM aerosol sizes are prescribed and are fixed both spatially and temporally, it is not surprising that this large discrepancy is observed. The validation against AERONET suggests that the GCM aerosol sizes are too large, especially for sulfate, nitrate, and carbonaceous aerosols that dominate urban regions. The low AE could also be associated with relatively high ambient relative humidity in the model, which leads to significant size growth of hygroscopic aerosols. Incorrect fraction of each aerosol species will also result in errors in AE. Comparison at each grid box (Figure 5) and global maps (figure not shown) supports the above results.

[24] The major sources of uncertainty in GCM aerosol simulation include aerosol and trace gas emission/reaction and transport from the chemical transport model, their optical property specification, size prescription, hygroscopicity parameterization, and ambient relative humidity. From the above comparison results, we consider aerosol size as the largest uncertainty in the current GCM aerosol simulation. Not only does it influence the AE but also it is related to AOD according to (1). In the next section, we will present results by allowing a spatially varying aerosol size field and optimal least squares fitting approach to achieve better agreement between the GCM aerosol climatology and AERONET. Nevertheless, further work is still needed to adjust the fraction of each aerosol component and to distinguish between fine and coarse modes.

## 5. Optimal Fitting of GCM Aerosol Climatology to AERONET Data

[25] The results of section 4 indicate significantly larger differences between GCM and AERONET AE. As a result, under the condition that aerosol mass density field has been specified by the chemical transport model, we consider

aerosol size specification as the largest source of uncertainty in the radiation model. In this section, we develop and apply an optimal fitting technique to GCM aerosol optical properties that matches model results with AERONET wavelength-dependent AOD and AE. The method seeks to minimize the MSE between GCM and AERONET AOD at all wavelengths, by adjusting aerosol size and solving for the “uncertainty parameter” that represents the combined error from other factors including Mie parameters, relative humidity, and mass density. For the moment, we are not able to quantify the individual error from each of these terms because of their complicated nature and lack of information.

### 5.1. Methodology

[26] For a certain GCM grid box that contains at least one AERONET station, the uncertainty of the model AOD at a certain wavelength is characterized by the MSE between the model seasonal cycle and AERONET data:

$$E_{\lambda} = \frac{\sum_{i=1}^n (\tau_{\text{mod}(i)} - \tau_{\text{aer}(i)})^2}{n}, \quad (4)$$

where  $E_{\lambda}$  is the MSE at wavelength  $\lambda$ ,  $\tau_{\text{mod}(i)}$  is the GCM AOD for month  $i$ ,  $\tau_{\text{aer}(i)}$  is AERONET observed AOD for month  $i$ , and  $n$  is total number of months that have available data. When the spectral dependence of AOD is taken into account, the combined uncertainty at all wavelengths, or “total MSE,” is expressed by a weighted average of  $E_{\lambda}$ . Because AODs at different wavelengths have different orders of magnitude, the weights assigned to each wavelength should be able to scale its  $E_{\lambda}$  to the same order of magnitude as the other wavelengths. In this study, we use the decycled variance of the AERONET AOD data at that wavelength and that grid box to normalize  $E_{\lambda}$ . The decycled variance can be calculated by removing the mean seasonal cycle from the AERONET data time series:

$$V_{\lambda} = \frac{\sum_{j=1}^m [\tau_{\text{aer}(j,im)} - \tau_{\text{ave}(im)}]^2}{m}, \quad (5)$$

where  $V_{\lambda}$  denotes the variance of AERONET AOD data.  $m$  is the total number of monthly mean data available at  $\lambda$ , for example, if there are 3 years of data,  $m = 36$ .  $\tau_{\text{aer}(j,im)}$  is a single AERONET data for the month  $im$  ( $im = 1, \dots, 12$ ). Last,  $\tau_{\text{ave}(im)}$  is the average AOD for the month  $im$ . The reason of

using  $V_\lambda$  as the weight is that it represents the variation scale of the data at that wavelength; thus, it can effectively normalize the data to approximately the same order of magnitude. Of course, there are other ways to normalize the data, such as taking the ensemble variance. However, as long as the normalization is effective, the method that is used should not affect the analysis results.

[27] Therefore, the total MSE for AOD at all wavelengths can be expressed as:

$$\text{TE} = \sum_{k=1}^w (E_{\lambda_k} / V_{\lambda_k}) \quad (6)$$

TE stands for total MSE,  $\lambda_k$  is the  $k$ th wavelength, and  $w$  is the total number of wavelengths. For most of the stations,  $w = 6$ . However, a few stations do not have data at certain channels, for example, data are not available at 340, 380, and 500 nm for Banizoumbou and Beijing, in which case  $w = 3$ .

[28] The optimal fitting should minimize TE by adjusting relevant parameters, among which the primary one is aerosol size. Considering the reasonable range and relatively low accuracy requirement for aerosol size, we treated it as a discrete variable taking values from  $0.1x$ ,  $0.2x$ , ...,  $1.2x$ , where  $x$  is the original size of each aerosol species. Dust sizes are not adjusted in this experiment because it already has seven size bins including fine and coarse modes. As a result, we have an ensemble of  $12^5$  size scenarios. However, because of other model uncertainties, either in the parameterization of the radiation model or in the mass density field from the chemical transport model, considerable disagreements are still observed between AOD after narrowing aerosol size uncertainty (figures not shown). As a result, we impose a parameter representing the combined effect of the other uncertainties to scale GCM AOD. Suppose after fitting,  $E_\lambda$  and TE become

$$E_\lambda = \frac{\sum_{i=1}^n [K\tau_{\text{mod}(i,r)} - \tau_{\text{aer}(i)}]^2}{n}, \quad (7)$$

where  $K$  is the uncertainty parameter of AOD,  $r$  is a certain size scenario, and is related to  $\tau$  according to (1), together with the relative humidity effect. For each size scenario,  $K$  is determined by minimizing its  $\text{TE}_{(r)}$ , i.e.,

$$\frac{\partial [\text{TE}_{(r)}]}{\partial K} = 0, \quad (8)$$

and solving for  $K$ . The group of size scenario and  $K$  that produces the smallest TE is then considered as optimal fitting parameters. This method is based on the relatively large uncertainty in aerosol size and good correlation between GCM and AERONET AOD seasonal cycle. The fitting is implemented grid box by grid box. Therefore, a geographically varying aerosol size and uncertainty parameter will be generated. For the moment, the temporal size variation is not allowed.

## 5.2 Results

[29] The optimal fitting has successfully reduced the TE. The spectral dependence of GCM AOD has been improved. Their magnitudes also match better with AERONET for most grid boxes.

[30] In Figure 3, we present scatterplots for the five aerosol types after the fitting. Compared with Figure 1, GCM AODs at all wavelengths have been greatly improved. The low bias is eliminated for biomass burning, rural, and urban aerosol regions. The high bias for dust and maritime aerosols has also been corrected. The correlation is also improved after the fitting. For example, over urban regions, the correlation coefficient has been raised from negative to more than 0.65. It should be noted that the optimal fitting technique seeks to minimize the total MSE at all available channels. Therefore, it is reasonable that results at certain channels may actually decay.

[31] Figure 4 displays the fitting results at the 15 selected grid boxes separately. For the dust sites, their AODs all matches well with AERONET after the fitting, with the GCM value varying within the  $\pm$ standard deviation of AERONET data (Figure 4, gray shades).

[32] The best-fitting results are achieved for the three biomass burning regions, namely, Alta\_Floresta, Mongu, and PCS, where both the seasonal variability and magnitude of the GCM AOD closely match those of AERONET at all wavelengths.

[33] For maritime aerosol, only Amsterdam\_Island agrees well with the AERONET after the fitting. The higher GCM AOD has been adjusted at Midway\_Island; however, there is still a 2 month phase shift in GCM seasonal cycle; that is, GCM AOD peaks in February and March, whereas AERONET AOD is highest in April and May. As for Tahiti, the two seasonal variations still disagree from January to May. In the GCM chemical transport model, sea-salt emission depends on wind speed. However, *Smirnov et al.* [2003] found that the correlation between aerosol optical parameters and wind speed are low for most island sites in the Pacific Ocean within the AERONET network. This indicates chemical transport simulation of sea salt need to be improved, particularly for the Pacific.

[34] The adjusted GCM AODs for rural and urban aerosols achieve excellent agreement with AERONET except for GCMSW. For this grid box, the summer AOD peak is still not well characterized. The results indicate that the seasonal cycles of black carbon and dust are simulated reasonably well, whereas the summer emission of the dominant species, namely, sulfate aerosols, requires to be further increased in the chemical transport model. Moreover, one limitation of this fitting approach is that the fraction of each aerosol species is not allowed to be adjusted, which makes it less effective at places where several aerosol species exist, such as the urban area. However, this problem usually requires tracing back to the chemical transport model, where we are able to adjust emissions and meteorology field to improve the results. Nonetheless, the fitting produced an optimal size combination and, to some extent, quantified the model uncertainty.

[35] As significant improvements have been achieved in AOD at all wavelengths for most grid boxes, similar results could be expected for the AE. The method greatly increased the correlation between GCM and AERONET 440/870 AE for biomass burning, maritime, urban, and rural aerosols (Figure 5). Because dust size is not adjusted in the current approach, the results for the three dust sites are not much improved. The AE at each grid box after the fitting is shown in Figure 6 (solid black lines). Ångström exponents at all grid boxes are increased and agree better with AERONET after the

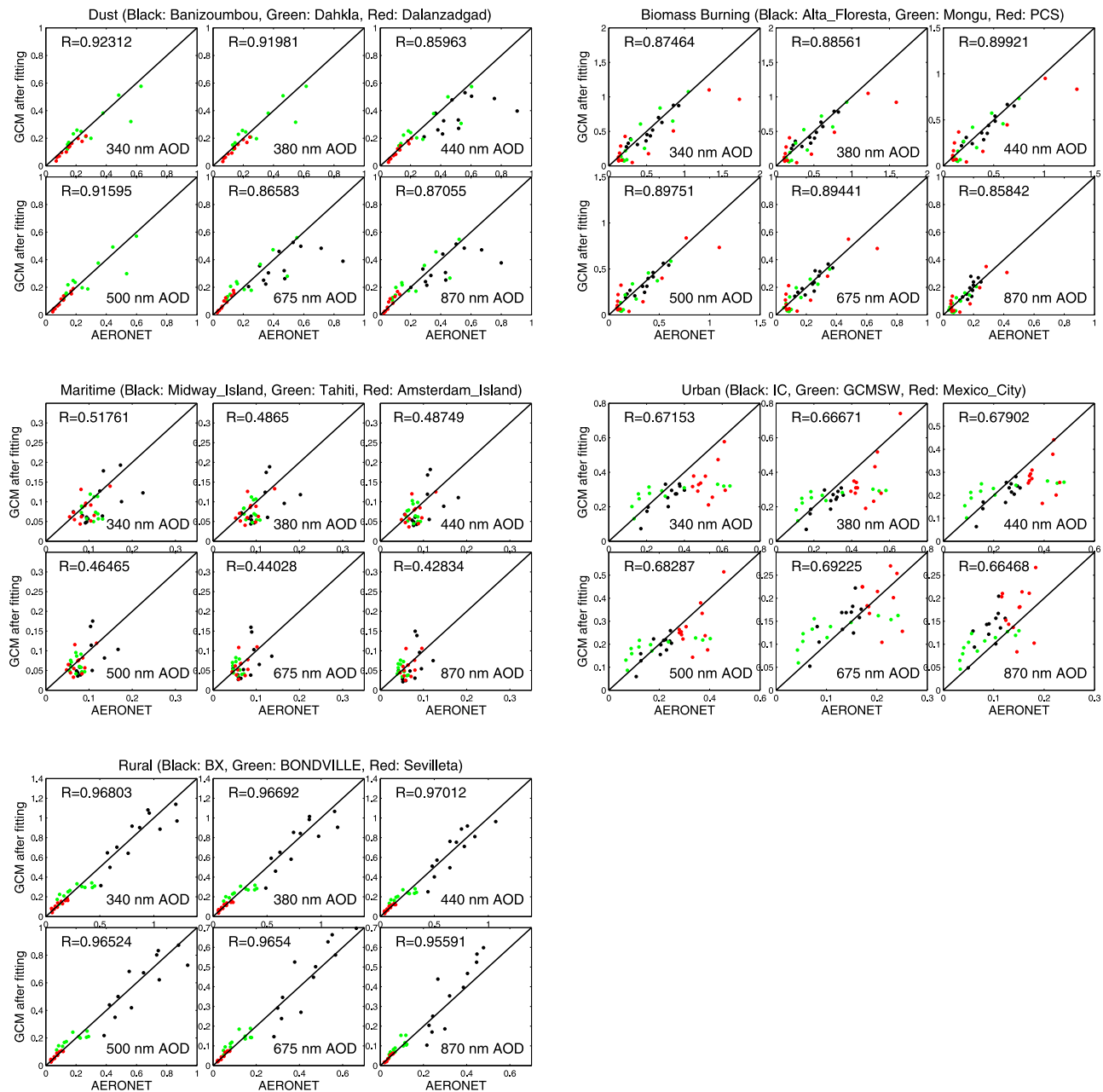


**Figure 3.** Scatterplots of AERONET and GCM AOD and ABS after fitting. The fitting successfully improved GCM AOD results for all aerosol types at all wavelengths. Comparatively large differences still exist for maritime aerosols, indicating problems in sea-salt seasonal variability. The ABS results are also improved but not as satisfying as AOD, partly because of the quality of AERONET inversion product.

fitting. Although the fitting does not include temporal variation of aerosol size, each aerosol species has its own seasonal variation, and adjusting their sizes also results in changes in the season cycle of AE. It is shown that seasonal cycles are also improved for most biomass burning, rural, and urban regions. In this study, the seven dust size bins are not adjusted, so dust AE is not significantly improved. Nevertheless, considerable differences are still observed for some grid boxes. For example, the GCM AE has a very different behavior from AERONET from April to October at Dalanzadgad. This suggests that, during this period, the region is characterized by smaller dust particles that the GCM

fails to capture. Sea salt sizes also remains problematic, especially for Tahiti. The current GCM assumes only one size mode for sea salt. However, its size can range from 0.03 to 8  $\mu\text{m}$  and has several modes [Gong *et al.*, 1997]. In future work, we will attempt to introduce more size modes to the GCM sea salt. The low GCM AE at urban areas indicates that the fraction of fine-mode aerosols, namely, sulfate, black carbon, and organic carbon, requires to be further adjusted.

[36] To sum up, our proposed optimal fitted approach by adjusting aerosol sizes and scale optical depth to minimize total MSE (TE) significantly improves GCM AOD magnitude, their spectral dependence, and seasonal variability for

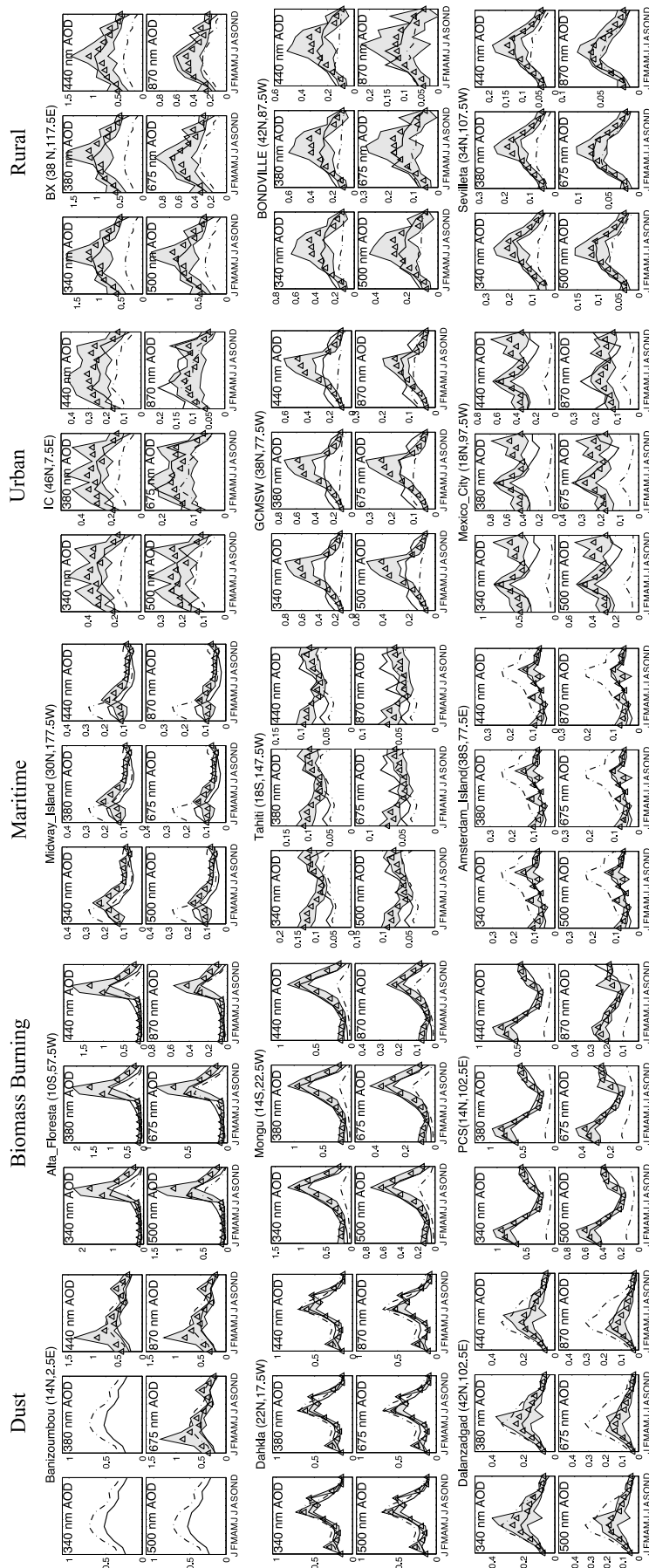


**Figure 4.** (triangle) The AOD at the six wavelengths for AERONET, (dashed black line) GCM before optimal fitting, and (solid black line) GCM after fitting. The gray-shaded area indicates  $\pm$ standard deviation of AERONET data. The AOD results well match AERONET data for most dust, biomass burning, urban and rural aerosols. Maritime aerosols still have phase differences in seasonal cycles, which require further inspection into the chemical transport mode.

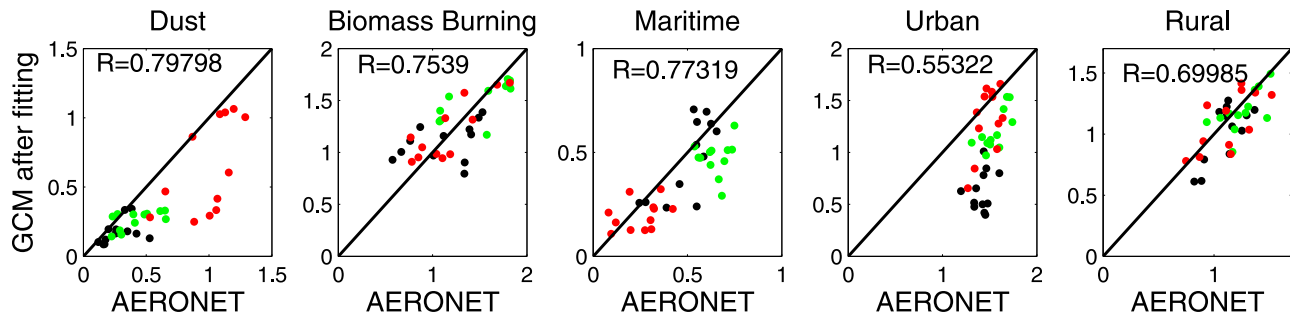


**Figure 5.** The fitting technique improves GCM AE results compared with Figure 2.

the five aerosol types. The results for the other grid boxes are similar, or even better (figures not shown). These preliminary results are encouraging in that they suggest that GCM aerosol climatology can be adjusted by this technique to yield better simulations. It also provides useful information to the upstream chemical transport model. Differences still exist after the fitting for some types of aerosol mainly because of the following:

[37] 1. A constant uncertainty parameter is applied to the total AOD, so the fraction of each aerosol species only changes slightly by adjusting their sizes. We have attempted to adjust the fraction of each aerosol species, through choosing an optimal combination of fraction multipliers from a certain interval (e.g., 0–3). However, because of the excess degrees of freedom, the fractions we obtained largely depend on the primarily defined interval, and the multipliers often lie on the boundaries, making the procedure less objective. Moreover, if we solve the six fractions pure mathematically using variation methods similar to (8), the results are sometimes unphysical (extremely large value or even negative). Additional information is required to constrain the fraction of each aerosol species;

[38] 2. Dust sizes are not adjusted, and the GCM has one mode for the other aerosol species. Anthropogenic aerosols such as sulfate, nitrate, black carbon, and organic carbon are usually smaller and can be treated as fine mode only. Sea salt size, however, requires a distribution with several modes [Gong *et al.*, 1997];

[39] 3. Here, we have 12 size scenarios for each aerosol component. The number and range can be further expanded to obtain better fitting results.

### 5.3. Optimally Fitted Sizes and Uncertainty Parameter

[40] After discussing the GCM results after the optimal fitting, in this section, we examine the aerosol sizes and the parameter representing model uncertainty that produce best fit.

[41] Table 2 lists the sizes and uncertainty parameter for the 15 grid boxes representing the five aerosol types.

[42] Despite a few individual differences, in general, we can conclude that dust has been overestimated by a factor of 0.6 to 0.8, organic carbon sizes should be decreased over biomass burning regions while black carbon size slightly increased, and the total AOD has been largely underestimated. Sea salt size should be increased, and AOD is overestimated; both urban and rural AODs have been underestimated by approximately a factor of 2, and the sizes

of dominant aerosol species (sulfate, nitrate, black carbon, and organic carbon) should be considerable reduced.

[43] In global distribution, Figure 7 shows the histogram of the fitted sizes and the uncertainty parameter. The size of organic carbon is reduced to 0.12 to 0.18  $\mu\text{m}$  for most places. Nitrate size is mostly reduced to 0.03  $\mu\text{m}$ . Sea salt sizes display an approximately bimodal distribution with two peaks at 0.2 and 1.2  $\mu\text{m}$ . This further supports the necessity of introducing more size modes for sea salt. Black carbon sizes have mostly been reduced to 0.03  $\mu\text{m}$ , corresponding to the majority of urban AERONET stations. The small peak at 0.12  $\mu\text{m}$  is produced by biomass burning regions. Sulfate aerosols have highly variable sizes and exhibit an approximate Gaussian distribution. Because of their various origins, such as fossil fuel burning, biomass burning, volcanoes, and biogenic, it is not out of expectation that sulfate aerosols have a broad size range. The uncertainty parameter mostly lies between 0 and 3 and peaks at bins 1 to 2. Because this parameter represents model errors from other sources in AOD, this distribution indicates that the model error is approximately a factor of 2.

[44] Except for sulfate sizes, the global distribution of the sizes and the uncertainty parameter shows distinct regional features (Figure 8). Organic carbon size has been uniformly decreased, and the biomass burning regions of South America, South Africa, and Southeast Asia have the smallest sizes (0.03  $\mu\text{m}$ ). Black carbon size is also decreased to below 0.03  $\mu\text{m}$  over urban and rural regions of North America, Europe, and Asia, but this is increased over biomass burning regions. The size of nitrate aerosols displays a similar distribution as black carbon. The size of sea salt mostly takes two extreme values. Large sizes (1.2  $\mu\text{m}$ ) are found over North America, Europe, East Asia, and all ocean grid boxes. Very small values (0.2  $\mu\text{m}$ ) appear over South America, South Africa, Sahara, Persian Gulf, and Central Asia, where sea-salt influence is insignificant. Sulfate size distribution is more complicated, but some regional characteristics can still be inferred. For example, the sizes over North America are mostly around 0.1  $\mu\text{m}$ , and over Europe and East Asia, the sizes are slightly larger, from 0.14 to 0.2  $\mu\text{m}$ . These approximately uniform regional size distributions is an encouraging result because it indicates the possibility to generate a regionally varying global size field that can be readily embedded into the GCM.

[45] The distribution of the uncertainty parameter can also be divided into regions dominated by different aerosol types. North African and Persian dust is reduced by a factor from 0.5 to 1. Biomass burning over South Africa, South America, and

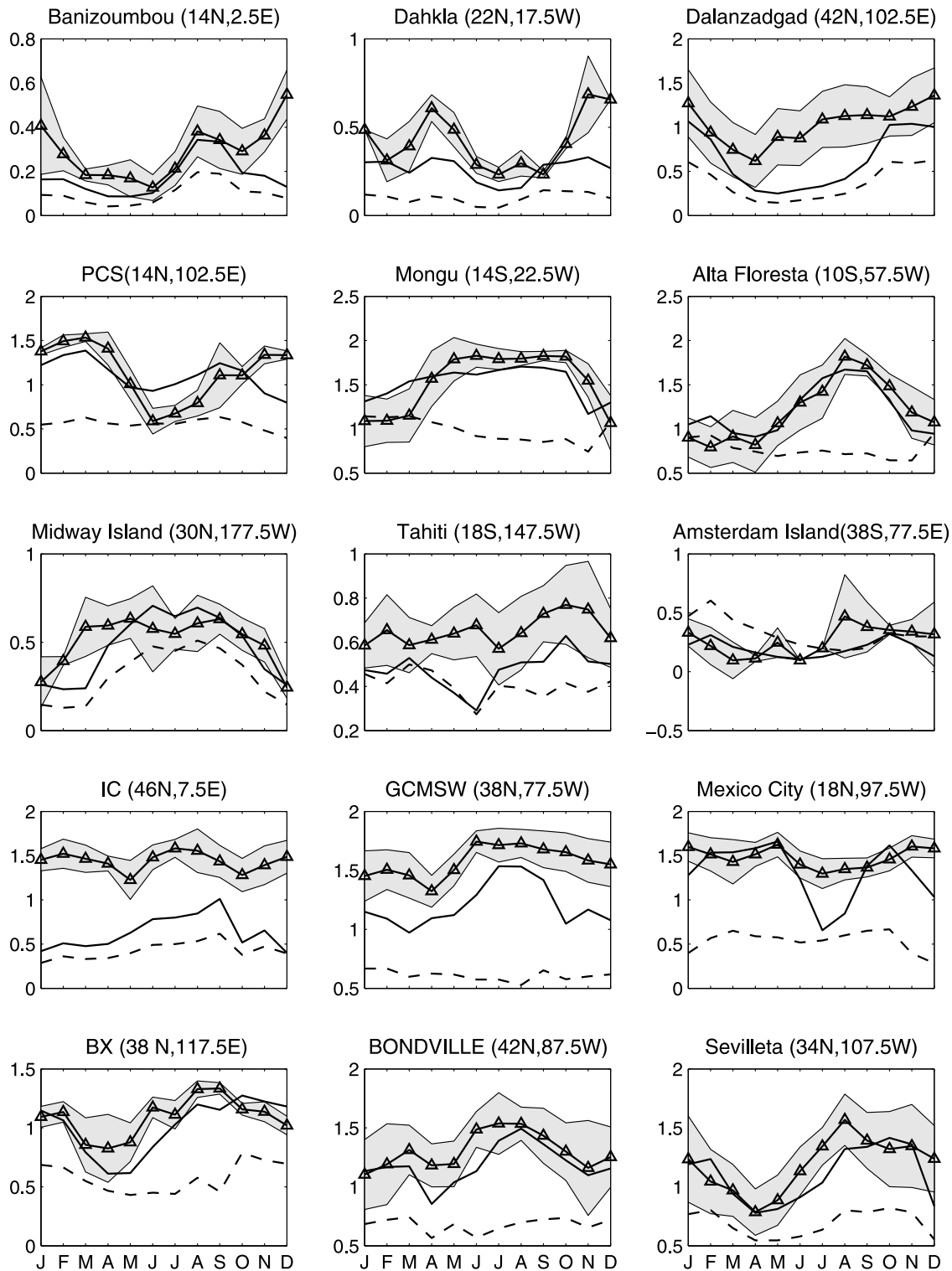


**Figure 6.** (triangle) The 440/870 ÅE for AERONET, (dashed black line) GCM before fitting, and (solid black line) GCM after fitting. Ångström exponent matches closer with AERONET after the fitting, indicating improvements in aerosol size specification. A few grid boxes still display relative large difference, for example, the summer months at Dalanzadgad, mainly because the seven dust sizes are excluded from the fitting. Disagreements over Tahiti during the summer might be associated with different sea-salt size modes. Moreover, the relatively low AE for urban aerosols may be caused by the fact that the fraction of each aerosol species is not adjusted without the presence of additional constraints.

**Table 2.** Fitted Sizes and Uncertainty Parameter for the 15 Selected Grid Boxes

Name	Fitted Sizes ( $\mu\text{m}$ )					$K$
	OC	NT	SS	BC	SU	
Banizoumbou	0.24	0.12	0.20	0.12	0.22	0.717
Dahkla	0.12	0.03	0.20	0.03	0.16	0.801
Dalanzadgad	0.12	0.12	0.10	0.03	0.10	0.612
PCS	0.12	0.03	10.1	0.12	0.12	4.614
Mongu	0.09	0.03	0.10	0.09	0.10	4.012
Alta_Floresta	0.18	0.15	10.0	0.12	0.18	1.496
Midway_Island	0.18	0.18	10.2	0.03	0.16	0.682
Tahiti	0.09	0.03	10.2	0.04	0.16	1.806
Amsterdam_Island	0.09	0.03	10.2	0.04	0.12	0.676
IC	0.12	0.03	10.2	0.03	0.10	2.070
GCMSW	0.12	0.03	10.2	0.04	0.14	2.268
Mexico_City	0.09	0.03	10.2	0.03	0.16	4.897
BX	0.12	0.21	10.1	0.05	0.14	2.297
BONDVILLE	0.15	0.03	10.2	0.11	0.12	2.280
Sevilleta	0.09	0.03	10.2	0.04	0.12	2.106

Southeast Asia is at least doubled and grew fourfold for a few grid boxes. The parameter varies around 1.5 over most urban and rural regions in North America, Europe, and East Asia. Overall, globally, the GCM underestimates aerosol optical properties by approximately a factor of 2, and the most serious underestimation occurs for biomass burning aerosols. *Sato et al.* [2003] concluded that the 1990 GCM aerosol climatology underestimates BC and OC by a factor of 2 to 2.5, inferred from the AERONET data. Our study supports this conclusion and suggests that this factor might be even higher at some locations after size adjustments.

[46] In sum, the GCM aerosol sizes and uncertainty parameter that yield optimal fitting show regionally uniform distributions, which is both realistic and easy to apply in the

model. In this way, we will be able to produce a geographically varying global aerosol size distribution. Moreover, on average, the GCM underestimates AOD at the selected grid boxes by approximately a factor of 2, with the largest underestimation associated with biomass burning. This factor may come from various aspects: mass density associated with emission and meteorology condition from the chemical transport model, aerosol Mie scattering parameter calculated from refractive indices, environmental relative humidity conditions and hygroscopic aerosol parameterization, aerosol internal mixing with other species, and errors from AERONET measurements. For the moment, it is beyond our scope to quantify the contribution from each of these factors. Large underestimation may be related to insufficient emission. Phase difference in seasonal cycle could be attributed to reversed local wind field. Moreover, low GCM absorption could result from incorrect organic carbon refractive indices and the absence of aerosol mixing. There is ongoing research to narrow the model uncertainty and to improve simulation results. Meanwhile, experiments will be carried out to apply the size and uncertainty parameter to the model and investigate the radiative and climate effects of aerosols.

## 6. Discussion

[47] An optimal fitting technique is development and used to improve GISS GCM aerosol climatology. The approach produced satisfying results for major aerosol types and constrained aerosol size for each species and model uncertainty. Especially, the adjusted aerosol sizes are consistent with model intercomparison results by *Kinne et al.* [2003], which suggests that the sulfate and carbonaceous aerosol sizes in the GISS model are large. In this study, the optimal fitting

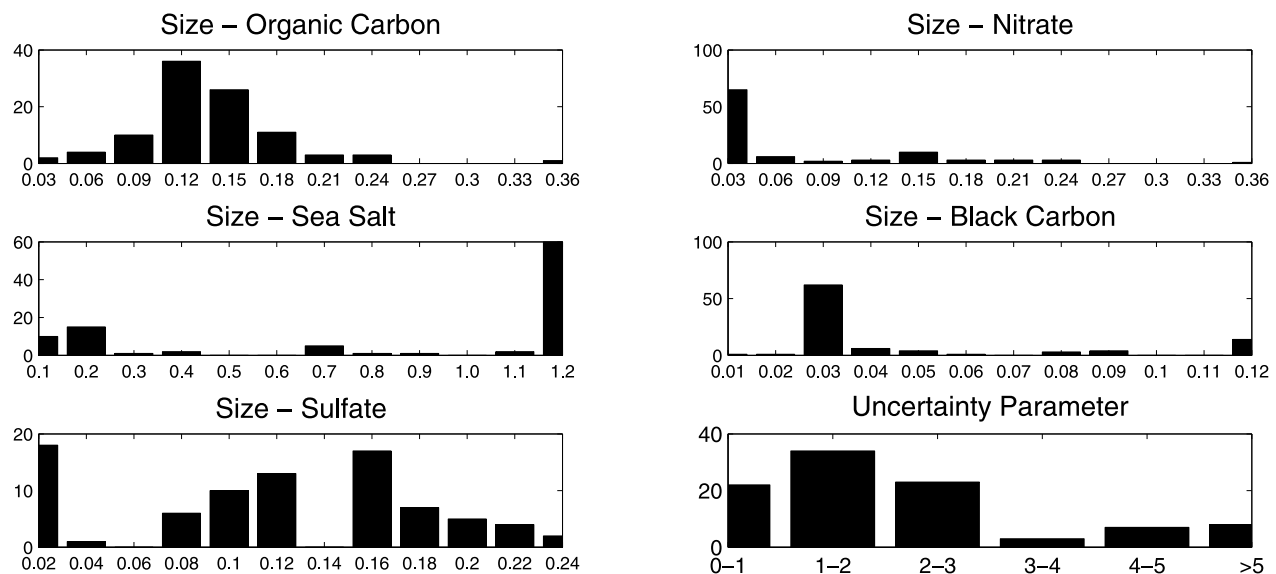


**Figure 7.** Histogram of organic carbon, nitrate, sea salt, black carbon, and sulfate aerosol size and the scaling factor (represents model uncertainty) that yield least squares fit. The sizes for organic carbon and nitrate are both significantly reduced. Sea-salt size shows a bimodal distribution with two central radii (0.2 and 1.2  $\mu\text{m}$ ). The 0.03  $\mu\text{m}$  peak for black carbon is associated with urban and rural regions, whereas the 0.12  $\mu\text{m}$  peak is associated with biomass burning aerosols. The size distribution for sulfate is broader. The uncertainty parameter concentrates within the 0 to 3 interval, and peaks in bins 1 to 2, indicating that overall GCM underestimates AOD by approximately a factor of 2.

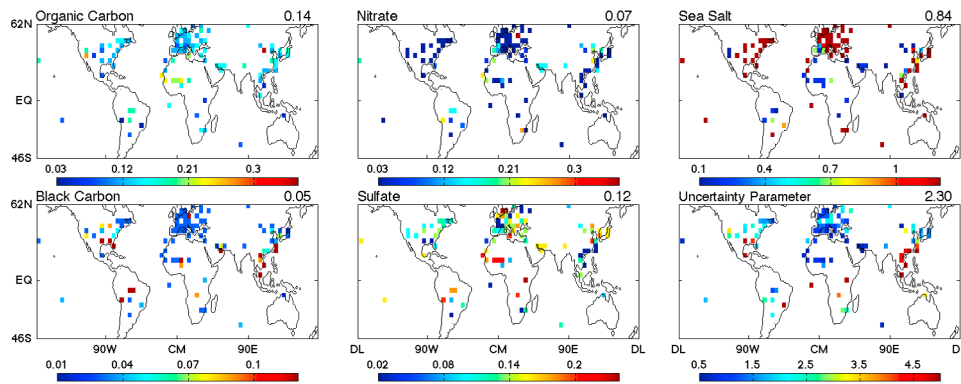


**Figure 8.** Global distribution of the optimal fitted sizes and uncertainty parameter. Except for sulfate, the sizes of the other four species all demonstrate regional characteristics; that is, the size is generally uniform within a certain spatial range. Smaller regions can also be identified in sulfate size map. The distribution of the uncertainty parameter indicates very low bias in GCM biomass burning simulation (as large as a factor of 5), underestimation in AOD over North America by a factor of 2, and a slight overestimation in dust.

approach produces reduced sulfate, black carbon, and organic carbon aerosol sizes. Considering that the uncertainty in dry size specification commonly exists in aerosol models, we suggest that the method could be extended to other models to improve their size parameterization. Compared with previous work of this kind by *Lesins and Lohmann* [2003], our work is initial; first, because we adjusted aerosol dry sizes of each aerosol species in an externally mixed aerosol module; and second, instead of using spectrally dependent AE, we used spectrally dependent AOD data. This potentially contains aerosol size information, as well as aerosol amount and their optical properties. Finally, in the least squares fitting process, we also quantified model uncertainty from other parameterization processes than size. However, currently, the method still has a few limitations.

[48] First, the comparisons and fitting technology are both performed in the radiation model, which only investigates problems involved in the mass density – optical property conversion process. This implicitly assumes a correct aerosol mass concentration simulation in the first place. However, this is not necessarily the case and can already be inferred from the results. In fact, sometimes, uncertainty in aerosol mass density is even larger than that in aerosol optical property calculation. For example, a fourfold underestimation in biomass burning aerosol AOD is likely the result of insufficient emission or excess removal, whereas the phase shift in sea-salt seasonal cycle might be attributed to incorrect wind field that generates an incorrect aerosol mass distribution. Therefore, further narrowing down model uncertainties requires investigation into the chemical transport model. *Koch et al.* [2009] evaluated black carbon in global aerosol models including GISS ModelE and also suggest an underestimation in column BC in biomass burning regions, and they infer that the chemical transport models may lack sufficient low-level pole-ward aerosol transport. Nevertheless, our work provides significant amount of information with regard to the chemical transport model. The authors will be collaborating with the GISS aerosol chemistry group to further improve aerosol simulation. Moreover, with improved aerosol mass density field, the fitting technique can again be performed to constrain aerosol size. This could be an iterative procedure until satisfying results are achieved.

[49] Second, on the one hand, the GCM aerosols are assumed to be externally mixed, with a single dry size prescribed to each species. On the other hand, the fraction of each aerosol species is not adjusted in this method because of the excess degrees of freedom as mentioned above. Therefore, the fine/coarse mode aerosol fraction can hardly be modified. The high spectral resolution of AERONET measurements helps to further examine this issue by providing additional information for the spectral dependence of AE. *Eck et al.* [1999] found significant curvature in the logarithm of aerosol optical depth versus logarithm of wavelength at AERONET stations characterized by biomass burning, urban, and dust aerosols. This results in a spectrally varying AE associated with the fraction of accumulation modes. *Schuster et al.* [2006] also used AERONET data to show that AEs at long wavelengths (0.67 and 0.87 nm) are sensitive to fine-mode volume fraction of aerosols, whereas AEs at short wavelengths (0.38 and 0.44 nm) are sensitive to fine-mode effective radius. *Kaskaoutis et al.* [2007] further investigated this relationship by studying data from four AERONET stations. They concluded that fine-mode particles exhibit negative curvature in the logarithm of AOD as a function of the logarithm of wavelength and have larger AEs at longer wavelength and vice versa. Here, we also present this relationship from a few selected grid boxes with largest disagreements to further evaluate the fitting results and to infer additional information (Figure 9). Ångström exponent is computed for four center wavelengths (380, 440, 500, and 675 nm) using a least squares fit to the three adjacent points. PCS, where biomass burning is dominant, clearly displays a change from winter coarse mode (positive curvature) to summer fine mode (negative curvature) in AERONET data. However, this reversal is not captured by the GCM. The GCM AE curvature is also completely different from AERONET at Midway Island. Similar phenomenon is observed for Tahiti. Introducing a bimodal sea salt size distribution will help to solve this problem. The January curve for Mexico\_City resembles AERONET, while the July curve differs. The AERONET curves suggest that this region is dominated by fine-mode particles during both seasons (larger AE at longer wavelength), which is reasonable over urban regions polluted by sulfate, nitrate, and carbonaceous aero-

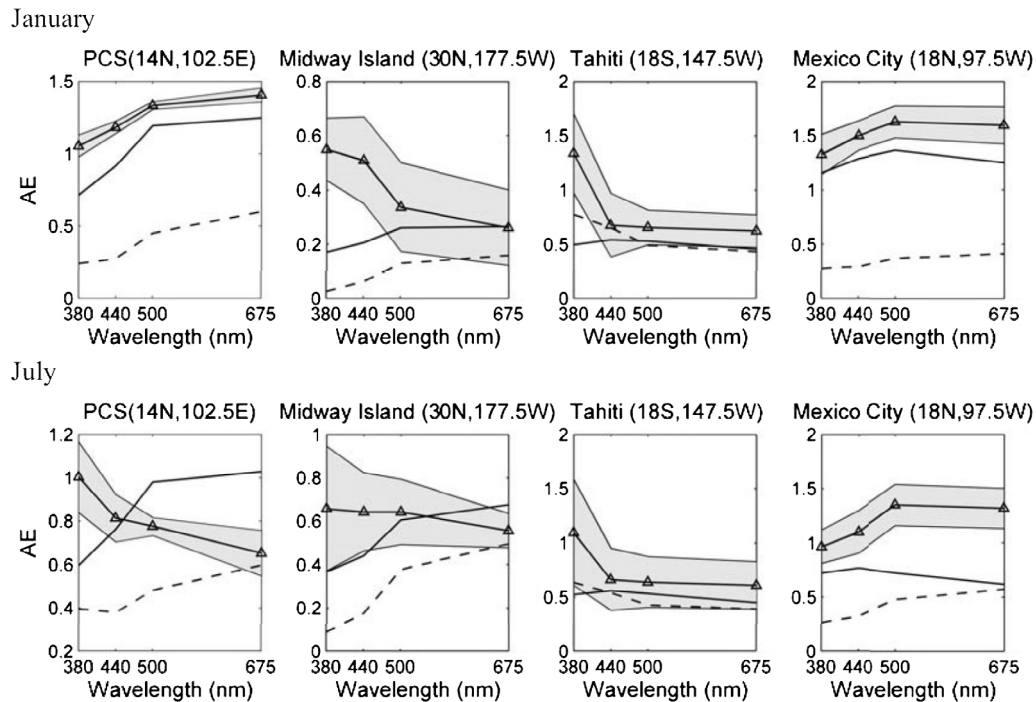


**Figure 9.** The dependence of AE on wavelengths for the selected grid boxes. This relationship is associated with fine/coarse mode's aerosol fraction and radius; thus, it can provide additional size information. The GCM AE spectral dependence is also improved by the fitting technique. However, GCM fails to capture aerosol size mode's seasonal reversal for Pimai and Midway\_Island and predicted incorrect size mode for Tahiti and Mexico\_City (summer).

sols. The GCM summer aerosol sizes need to be further considered in future work.

[50] Third, in addition to directly measured aerosol extinction (AOD), AERONET also provides inversion products such as ABSorption optical depth (ABS). These data provide possibilities to further constrain absorbing aerosols, i.e., black carbon, dust, and organic carbon aerosols. *Sato et al.* [2003] used AERONET aerosol absorption optical depth to calibrate global black carbon climatology in the previous version (1990 aerosol climatology) of GISS GCM and found that the GCM BC must be increased by a factor of 2 to 4. Here, we also compare the 440, 675, and 870 nm ABS between AERONET and GCM at selected dust and biomass burning locations. The GCM ABS is simulated similar to AOD but replacing  $Q_{\text{ext}}$  with  $(Q_{\text{ext}} - Q_{\text{sct}})$  in equation (1), where  $Q_{\text{sct}}$  is scattering efficiency. Again, only clear-sky data are used to be consistent with AERONET measurements. In the updated GISS GCM aerosol climatology, aerosol absorption is still underestimated at biomass burning locations (Figure 10). The reasons could be insufficient aerosol loading, insufficient absorption especially from organic carbon aerosols, and lack of aerosol mixing. It has been shown that the coating of organic carbon on black carbon will significantly increase the absorption of black carbon (K. Tsigaridis, personal communication, 2008). We have also extended the optimal fitting technique to include ABS at the three wavelengths. After fitting, the GCM ABS well matches AERONET for the biomass burning locations of Mongu and PCS (Figure 10, solid black lines). For Banizoumbou and Dahkla, where dust aerosol dominates, the

GCM ABS seasonal cycles differ from AERONET in both the magnitude and the phase. Even optimal fitting does not show evident improvements. However, it is questionable that the AERONET ABS seasonal cycles do not agree with AOD at these two locations. To further investigate this, we introduce the aerosol index (AI) product from TOMS, which is a qualitative measurement of aerosol absorption. Version 8 AI is defined as:

$$\text{AI} = -100 \left[ \log_{10} (I_{331/360})_{\text{meas}} - \log_{10} (I_{331/360})_{\text{calc}} \right], \quad (9)$$

where  $I_{\text{meas}}$  is the measured backscattered radiance at a given wavelength and  $I_{\text{calc}}$  is the backscattered radiance calculated at that wavelength for a pure Rayleigh atmosphere.

[51] Thus, by this definition, AI is positive for UV absorbing aerosols, near zero for clouds, and negative for scattering aerosols [Torres et al., 1998]. Here, we use version 8 monthly mean  $1^\circ \times 1.25^\circ$  AI product from Earth Probe TOMS from 1997 to 2000. To compare with GCM, we compute the overall monthly mean and rescale the data to GCM resolution ( $4^\circ \times 5^\circ$ ). We find that the seasonal correlation between GCM ABS and TOMS AI (thick gray line on 440 nm ABS panel) are high at Banizoumbou and Dahkla (0.84 and 0.98, respectively), while that between AI and AERONET are much lower (0.48 and 0.36, respectively). The correlation between GCM ABS and AERONET ABS are similar to that between AI and AERONET ABS. For one thing, this might indicate that this one AERONET station is not sufficient to represent the whole GCM grid box. For the

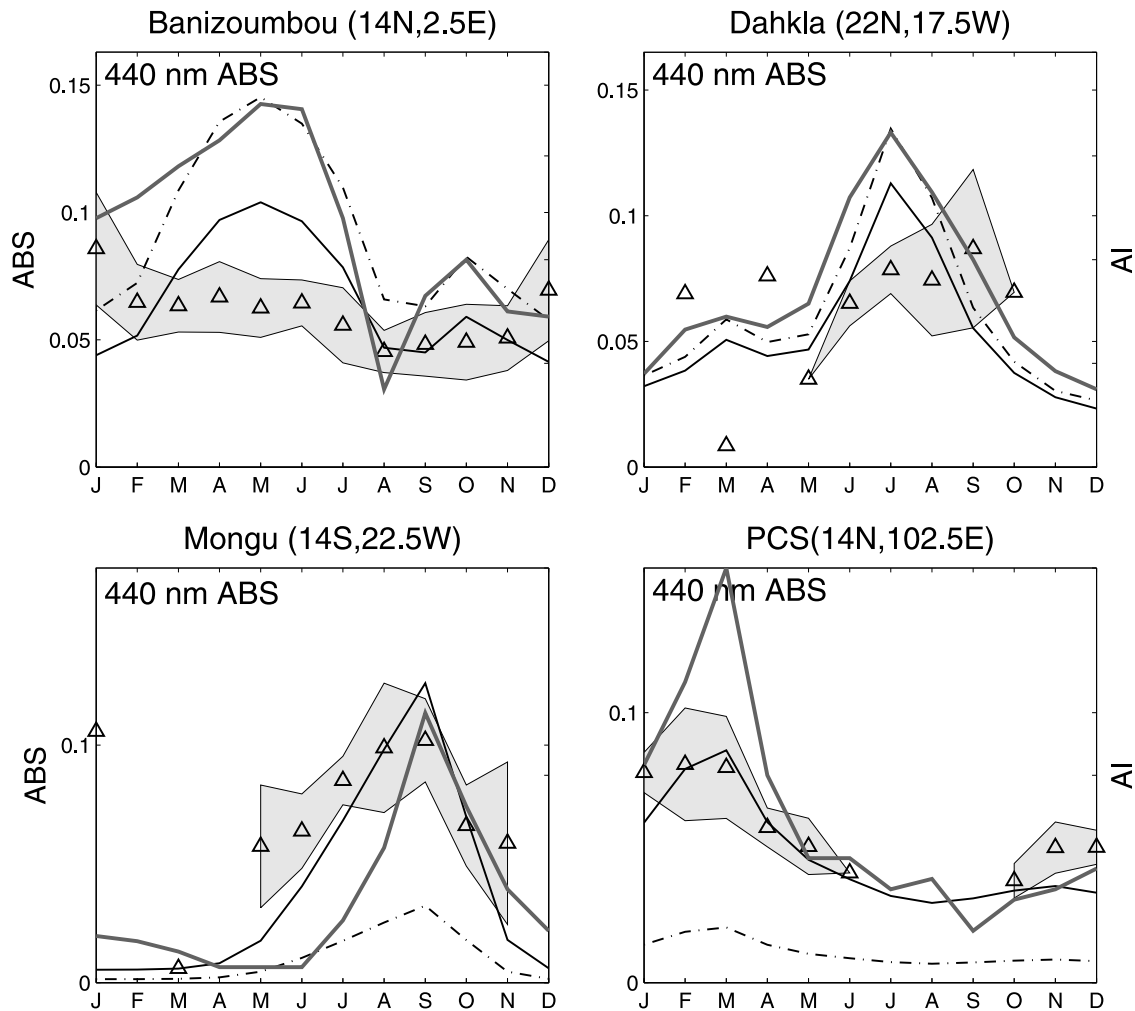


**Figure 10.** Aerosol absorption optical depth at 440 nm for the selected grid boxes: (triangle) AERONET, (dashed black line) GCM before fitting, and (solid black) GCM after fitting. The shaded area indicates  $\pm$ standard deviation of AERONET data. In addition, the TOMS AI data are indicated by the thick gray line. The TOMS AI seasonal cycle does not agree with that of AERONET ABS but agrees with the GCM for dust aerosols, which might be because of the inaccuracy in aerosol shape assumption in AERONET's inversion for dust. The seasonal cycle of GCM ABS agrees well with AERONET for biomass burning aerosols, and after the fitting, the GCM ABS closely matches the AERONET data.

other, AERONET inversion products have sources of uncertainty from Sun or sky channel miscalibration, inaccurate azimuth angle pointing during sky radiance measurements, inaccuracy in accounting for surface [Dubovik *et al.*, 2000], and errors from assumed aerosol shape, especially for dust stations. Because of the disagreement between AERONET ABS and TOMS AI, we suspect that the accuracy and quality of the AERONET ABS product is less than those of AERONET AODs. For this work, our fitting is mainly based on the AOD measurements.

[52] Fourth, currently AERONET ground measurements are considered to be the most suitable data set to validate aerosol models. The AERONET network measures spectral extinction by aerosols from direct beam observations of the sun, with high spectral and time resolution [Eck *et al.*, 1999]. It provides both high-quality data and additional spectral information associated with aerosol size and composition. However, AERONET data have the limitation of sparse

spatial coverage and bias caused by daytime and clear-sky sampling. Kinne *et al.* [2003] discussed the potential problems in temporal and regional representation of AERONET data. Moreover, AERONET and most satellite retrievals only measure column-integrated quantities, whereas the vertical structure of aerosols (especially absorbing aerosols) also plays important roles in their climate effects. In the future, with the extension of the AERONET network, more accurate and comprehensive validation of aerosol models will be possible.

[53] Finally, the different time periods for model simulation and measurement and not real-time wind field that drives aerosol distribution in the model could also contribute to the disagreements between the fitted results and AERONET data.

[54] In sum, although the fitting approach generated the "optimal" sizes and uncertainty parameters, we regard the results to be more qualitative than quantitative. We are more confident in the sign of the adjustment (i.e., increase or decrease, overestimate or underestimate) rather than the

absolute magnitude. The essence of the fitting not only is confined to improving GCM results but also lies in the potential information revealed in this process. The scheme can be further improved by extending size scenarios and introducing additional constraints to adjust the fraction of each aerosol species. Its usage can also be easily extended to other aerosol model results or using other observation data sets.

## 7. Summary and Conclusions

[55] In this paper, we improve the GISS ModelE aerosol optical properties on the basis of the comparisons with AERONET ground measurements. With AOD data available from six wavelengths, we construct an “AERONET simulator” within the GCM to produce the corresponding clear-sky aerosol optical properties. First, comparisons are performed on the magnitude and seasonal cycles of AOD and its spectral dependences, and AE, focusing on regions dominated by five aerosol types. The results reveal that the GCM underestimates the loading of biomass burning, urban, and rural aerosols, whereas it slightly overestimates dust and sea-salt aerosols. The GCM AOD achieves fairly high seasonal correlation with AERONET for dust, biomass burning, and rural aerosols. Moreover, the GCM has a flatter AOD spectral dependence, thus a low biased AE. The temporal variability of AE is also poorly represented. Global comparison is consistent with the 15 selected grid boxes by aerosol type.

[56] On the basis of the above results, we identify size prescription as the primary source of uncertainty in the radiation model of aerosol simulation. An optimal least squares fitting technique is developed accordingly to constrain dry sizes for sulfate, nitrate, black carbon, organic carbon, and sea-salt aerosols assuming completely external mixing and to quantify the combined error resulting from other factors including Mie parameter, ambient relative humidity, aerosol mass concentration, and so on. The goal of the fitting is to minimize total normalized MSE (TE) at the six AOD wavelengths. The results show considerable improvements in the magnitude and seasonal cycles of GCM AOD and AE. The best fitting is achieved for biomass burning, dust, and rural aerosols. Differences still exist for urban and maritime aerosols. These problems require further adjustments in the upstream conditions, such as emission and transport in the chemical transport model, rather than in the radiative transfer model that this study focused on. The distribution of sizes and uncertainty parameter that yield best fit indicates that the organic carbon sizes should be reduced to 0.12 to 0.15  $\mu\text{m}$ , nitrate reduced to 0.03  $\mu\text{m}$ , black carbon also reduced to 0.03  $\mu\text{m}$  for urban and rural areas but that these should be slightly increased for biomass burning regions. Sea salt size has a bimodal distribution, with centers at 0.2 and 1.2  $\mu\text{m}$ . Sulfate size is highly variable, and the distribution is approximately Gaussian. From the uncertainty parameter, we infer that biomass burning aerosols (organic and black carbon) have been underestimated by a factor as large as 4, urban and rural aerosols are underestimated by approximately a factor of 2 over North America and around 1.5 over Europe, while there is a slight overestimation in dust and maritime aerosols. The global pattern of the parameters display some encouraging regional characteristics, based on which it will be possible to generate a regionally varying aerosol size data

set in the GCM, which is one of the topics of our future study. Further attempts will also be made to adjust dust size in the dust model, introducing new Mie parameters for organic carbon and improving aerosol processes in the chemical transport model such as aerosol emission, transport, mixing, and microphysics.

[57] **Acknowledgments.** The authors thank the AERONET team for providing the ground-based Sun photometer data used in this study. The authors also thank the TOMS team for providing the AI product. The authors also thank Dorothy Koch, Susanne Bauer, and Konstantinos Tsigaridis for providing valuable information and advice regarding GISS chemical transport model and aerosol processes.

## References

- Andreae, M. O., and P. Merlet (2001), Emission of trace gases and aerosols from biomass burning, *Global Biogeochem. Cycles*, *15*(4), 955–966, doi:10.1029/2000GB001382.
- Bauer, S. E., D. Koch, N. Unger, S. M. Metzger, D. T. Shindell, and D. G. Streets (2007), Nitrate aerosols today and in 2030: A global simulation including aerosols and tropospheric ozone, *Atmos. Chem. Phys.*, *7*, 5043–5059.
- Bond, T. C., D. G. Streets, K. F. Yarber, S. M. Nelson, J.-H. Woo, and Z. Klimont (2004), A technology-based global inventory of black and organic carbon emissions from combustion, *J. Geophys. Res.*, *110*, D14203, doi:10.1029/2003JD003697.
- Dubovik, O., A. Smirnov, B. N. Holben, M. D. King, Y. J. Kaufman, T. F. Eck, and I. Slutsker (2000), Accuracy assessments of aerosol optical properties retrieved from AERONET Sun and sky-radiance measurements, *J. Geophys. Res.*, *105*(D8), 9791–9806, doi:10.1029/2000JD900040.
- Eck, T. F., B. N. Holben, J. S. Reid, O. Dubovik, A. Smirnov, N. T. O'Neill, I. Slutsker, and S. Kinne (1999), Wavelength dependence of the optical depth of biomass burning, urban, and desert dust aerosols, *J. Geophys. Res.*, *104*(D24), 31,333–31,349, doi:10.1029/1999JD900923.
- Gong, S. L., L. A. Barrie, and J.-P. Blanchet (1997), Modeling sea salt aerosols in the atmosphere: 1. Model development, *J. Geophys. Res.*, *102*(D3), 3805–3818, doi:10.1029/96JD02953.
- Hansen, J. E., and L. D. Travis (1974), Light scattering in planetary atmospheres, *Space Sci. Rev.*, *16*, 527–610.
- Hansen, J., M. Sato, R. Ruedy, A. Laics, and V. Oinas (2000), Global warming in the twenty-first century: An alternative scenario, *Proc. Natl. Acad. Sci. U. S. A.*, *97*, 9875–9880.
- Hansen, J., et al. (2002), Climate forcings in Goddard Institute for Space Studies S12000 simulations, *J. Geophys. Res.*, *107*(D18), 4347, doi:10.1029/2001JD001143.
- Holben, B. N., et al. (1998), AERONET – A federated instrument network and data archive for aerosol characterization, *Remote Sens. Environ.*, *66*, 1–16.
- Intergovernmental Panel on Climate Change (2001), *Climate Change 2001: The Scientific Basis*, edited by J. T. Houghton et al., Cambridge Univ. Press, New York.
- Kaskaoutis, D. G., H. D. Kambezidis, N. Hatzianastassiou, P. G. Kosmopoulos, and K. V. S. Badarinath (2007), Aerosol climatology: Dependence of the Ångström exponent on wavelength over four AERONET sites, *Atmos. Chem. Phys. Disc.*, *7*, 7374–7397.
- Kinne, S. (2008), Aerosol direct radiative forcing with an AERONET touch, *Atmos. Environ.*, in press.
- Kinne, S., et al. (2003), Monthly averages of aerosol properties: A global comparison among models, satellite data, and AERONET ground data, *J. Geophys. Res.*, *108*(D20), 4634, doi:10.1029/2001JD001253.
- Koch, D. (2001), Transport and direct radiative forcing of carbonaceous and sulfate aerosols in the GISS GCM, *J. Geophys. Res.*, *106*, 20,311–23,332, doi:10.1029/2001JD900038.
- Koch, D., G. A. Schmidt, and C. V. Field (2006), Sulfur, sea salt, and radionuclide aerosols in GISS ModelE, *J. Geophys. Res.*, *111*, D06206, doi:10.1029/2004JD005550.
- Koch, D., T. C. Bond, D. Streets, N. Unger, and G. R. van der Werf (2007), Global impacts of aerosols from particular source regions and sectors, *J. Geophys. Res.*, *112*, D02205, doi:10.1029/2005JD007024.
- Koch, D., et al. (2009), Evaluation of black carbon estimations in global aerosol models, *Atmos. Chem. Phys. Disc.*, *9*, 15,769–15,825.
- Lacis, A. A., and M. I. Mishchenko (1995), Climate forcing, climate sensitivity, and climate response: A radiative modeling perspective on atmo-

- spheric aerosols, in *Aerosol Forcing of Climate*, edited by R. J. Charlson and J. Heintzenger, pp. 11–42, John Wiley, Hoboken, N. J.
- Lesins, G., and U. Lohmann (2003), GCM aerosol radiative effects using geographically varying aerosol sizes deduced from AERONET measurements, *J. Atmos. Sci.*, *60*, 2747–2764.
- Lesins, G., and U. Lohmann (2005), Using MODIS and AERONET to determine GCM aerosol size, *J. Atmos. Sci.*, *63*, 1338–1347.
- Liu, L., and M. I. Mishchenko (2008), Toward unified satellite climatology of aerosol properties: Direct comparisons of advanced level 2 aerosol products, *J. Quant. Spectrosc. Radiat. Transfer*, *109*, 2376–2385, doi:10.1016/j.jqsrt.2008.05.003.
- Liu, L., A. A. Lacis, B. E. Carlson, M. I. Mishchenko, and B. Cairns (2006), Assessing Goddard Institute for Space Studies ModelE aerosol climatology using satellite and ground-based measurements: A comparison study, *J. Geophys. Res.*, *111*, D20212, doi:10.1029/2006JD007334.
- Miller, R. L., et al. (2006), Mineral dust aerosols in the NASA Goddard Institute for Space Studies Sciences ModelE atmospheric general circulation model, *J. Geophys. Res.*, *111*, D06208, doi:10.1029/2005JD005796.
- Mishchenko, M. I., et al. (2007), Past, present, and future of global aerosol climatologies derived from satellite observations: A perspective, *J. Quant. Spectrosc. Radiat. Transfer*, *106*, 325–347.
- Monahan, E. C., D. E. Spiel, and K. L. Davidson (1986), A model of marine aerosol generation via whitecaps and wave disruption, in *Oceanic Whitecaps*, edited by E. C. Monahan and G. Mac Niocaill, pp. 167–174, Springer, New York.
- Sato, M., J. Hansen, D. Koch, A. Lacis, R. Ruedy, O. Dubovik, B. Holben, M. Chin, and T. Novakov (2003), Global atmospheric black carbon inferred from AERONET, *Proc. Natl. Acad. Sci. USA*, *100*, 6319–6324.
- Schmidt, G. A., et al. (2006), Present-day atmospheric simulations using GISS ModelE: Comparison to in-situ, satellite and reanalysis data, *J. Clim.*, *19*, 153–192, doi:10.1175/JCLI3612.1.
- Schuster, G. L., O. Dubovik, and B. N. Holben (2006), Ångström exponent and bimodal aerosol size distributions, *J. Geophys. Res.*, *111*, D07207, doi: 10.1029/2005JD006328.
- Smirnov, A., et al. (2000), Cloud screening and quality control algorithms for the AERONET database, *Remote Sens. Environ.*, *73*, 334–337.
- Smirnov, A., B. N. Holben, T. F. Eck, O. Dubovik, and I. Slutsker (2003), Effect of wind speed on columnar aerosol optical properties at Midway Island, *J. Geophys. Res.*, *108*(D24), 4802, doi:10.1029/2003JD003879.
- Tang, I. N. (1996), Chemical and size effects of hygroscopic aerosols on light scattering coefficients, *J. Geophys. Res.*, *101*(D14), 19,245–19,250, doi:10.1029/96JD03003.
- Tang, I. N., and H. R. Munkelwitz (1991), Simultaneous determination of refractive index and density of an evaporating aqueous solution droplet, *Aerosol Sci. Technol.*, *15*, 201–207.
- Tang, I. N., and H. R. Munkelwitz (1994), Water activities, densities, and refractive indices of aqueous sulfates and sodium nitrate droplets of atmospheric importance, *J. Geophys. Res.*, *99*(D9), 18,801–18,808, doi:10.1029/94JD01345.
- Textor, C., et al. (2006), Analysis and quantification of the diversities of aerosol life cycles within AeroCom, *Atmos. Chem. Phys.*, *6*, 1777–1813.
- Torres, O., P. K. Bhartia, J. R. Herman, Z. Ahmad, and J. Gleason (1998), Derivation of aerosol properties from satellite measurements of backscattered ultraviolet radiation: Theoretical basis, *J. Geophys. Res.*, *103*(D14), 17,099–17,110, doi:10.1029/98JD00900.
- Wagner, F., and A. M. Silva (2008), Some considerations about Ångström exponent distributions, *Atmos. Chem. Phys.*, *8*, 481–489.

B. E. Carlson, A. A. Lacis, and L. Liu, NASA Goddard Institute for Space Studies, 2880 Broadway, New York, NY 10025-7886, USA.

J. Li, Department of Earth and Environmental Sciences, Columbia University, 2800 Broadway, New York, NY 10025, USA. (jli@giss.nasa.gov)